

# Online Video Quality Enhancement with Spatial-Temporal Look-up Tables

Zefan Qu<sup>1</sup>, Xinyang Jiang<sup>2</sup>, Yifan Yang<sup>2</sup>, Dongsheng Li<sup>2</sup>, and Cairong Zhao<sup>1</sup>

<sup>1</sup> Tongji University, Shanghai, China

<sup>2</sup> Microsoft Research Asia, Shanghai, China

{qzf, zhaocairong}@tongji.edu.cn

{xinyangjiang,yifanyang,dongsheng.li}@microsoft.com

**Abstract.** Low latency rates are crucial for online video-based applications, such as video conferencing and cloud gaming, which make improving video quality in online scenarios increasingly important. However, existing quality enhancement methods are limited by slow inference speed and the requirement for temporal information contained in future frames, making it challenging to deploy them directly in online tasks. In this paper, we propose a novel method, STLVQE, specifically designed to address the rarely studied online video quality enhancement (Online-VQE) problem. Our STLVQE designs a new VQE framework which contains a Module-Agnostic Feature Extractor that greatly reduces the redundant computations and redesign the propagation, alignment, and enhancement module of the network. A Spatial-Temporal Look-up Tables (STL) is proposed, which extracts spatial-temporal information in videos while saving substantial inference time. To the best of our knowledge, we are the first to exploit the LUT structure to extract temporal information in video tasks. Extensive experiments on the MFQE 2.0 dataset demonstrate our STLVQE achieves a satisfactory performance-speed trade-off.

**Keywords:** Online Video Quality Enhancement · Look-up Table · Video Compression Artifact Reduction

## 1 Introduction

With the rapid development of social media, users are increasingly seeking high-quality and real-time video content. In recent times, video-based applications such as video conferencing, webcasting, and cloud gaming have increasingly demanded low latency requirements. This has resulted in higher video compression rates, which can cause a noticeable decrease in video quality and an overall reduction in the Quality of Experience (QoE). As a result, online Video Quality Enhancement (Online-VQE), which improves the quality of real-time streaming video under online conditions and minimizing video defects caused by compression algorithms (e.g., H.264/AVC [27] and H.265/HEVC [24]) has become a significant problem. However, Online-VQE poses two main challenges compared to the conventional offline VQE approach. Firstly, it needs to process

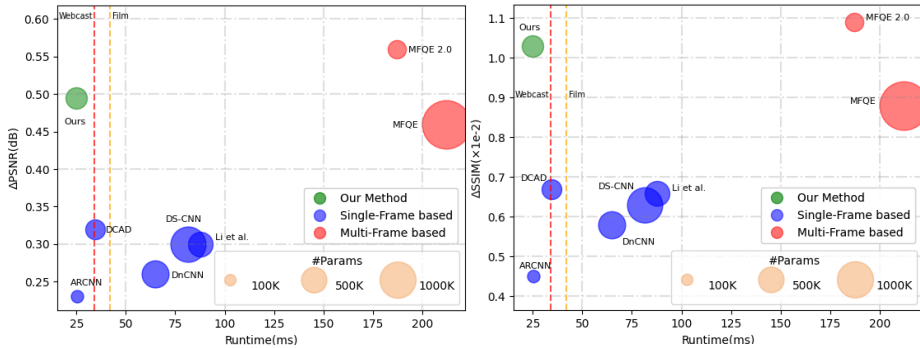


**Fig. 1:** Comparison of  $\Delta$ PSNR/ $\Delta$ SSIM, average runtime per frame(720P video) and parameters on MFQE 2.0 test set at QP=37. Our STLVQE method achieves a great trade-off in enhancement performance and inference speed.

high-resolution videos in real-time to ensure a smooth viewing experience. Secondly, online video processing techniques [15, 18, 22] can only rely on the current and previous frames for inference due to the uncontrolled latency caused by waiting for future frames, which can result in overall video delay.

In recent years, numerous neural network-based techniques for enhancing the quality of compressed video have been developed, resulting in significant advancements in this field. These methods can be broadly classified into two categories, namely single-image based VQE method [4, 12, 29, 30] and multi-frame based VQE method [2, 6, 10, 20, 36]. Single-image based approaches are relatively faster in inference speed, but they ignore the significance of temporal information in video [31]. On the other hand, multi-frame based VQE achieves state-of-the-art performance by utilizing temporal information. However, most of these approaches are not suitable for online scenarios because they rely on subsequent frames as reference frames and have un-satisfactory inference speeds. Therefore, developing a new online-VQE method that satisfies the aforementioned two constraints while effectively leveraging temporal information is essential.

Reasons that limit the speed and latency of the above temporal VQE methods can be summarized in the following two points: First, a high level of computational redundancy exists within these methods, and these homogeneous computations increase the network’s inference time. Second, most of these methods employ complex and computationally intensive models, which sacrificing inference speed and latency for some of the enhancement capabilities. In this work, a more applicable VQE method for online scenarios are proposed by advancing these two perspectives.

As discussed in previous works [1], modern VQE methods exploit temporal information by constructing a neural network containing three main components: the propagation, alignment and enhancement module. In all three modules, similar feature extraction operations on the original image may be involved, e.g., the reference frame selection [10, 31] in propagation module, the optical flow

calculation [1, 2] in alignment module and the final result obtaining in the enhancement module [6, 10]. Most of the state-of-the-art methods adopts distinct feature extractors in different components and obtaining latent feature for each component separately, causing large computation redundancy. In this paper, we design a new VQE network framework containing a Module-Agnostic Feature Extractor (MAFE), where the extracted latent feature are uniformly share across three modules. This design allows the network to greatly reduce the redundant feature computation steps and speed up the inference of the network.

When processing high-resolution videos in VQE task, the complex network of the sota method will greatly increase the computation times of the network, thus affecting the online deployment of the method. Therefore, we in our proposed framework: (1) Redesign the structure of the three modules with a light-weight convolutional structure. (2) Propose a Spatial-Temporal Look-up Tables (ST-LUTs) that extend conventional LUTs [13] to conduct queries on both spatial and temporal dimensions, which allows the LUTs to simultaneously capture information in both temporal and spatial dimensions, facilitating efficient extraction of temporal information. To the best of our knowledge, ST-LUTs is the first approach to employ a LUT structure for the extraction of temporal information.

The major contributions are summarized as follows: (1) We propose the first online-VQE method STLTVQE that achieves real-time process speed, which reduces redundant feature extraction computations while redesigning the propagation, alignment and enhancement modules of the temporal VQE network. (2) A Spatial-Temporal Look-up Tables structure is first time proposed for fully exploiting the temporal and spatial information in the video. (3) Extensive experiments on MFQE 2.0 dataset demonstrate that our approach achieves a comparable speed-performance trade-off. We also test most of the previous VQE methods on prevalent GPU to provide performance and speed benchmarks, facilitating future research in this area.

## 2 Related Works

**Compressed Video Quality Enhancement.** Recently, numerous works have focused on the degradation of the network video quality due to the lossy video compression algorithms. Existing Compressed VQE work can be broadly classified into two categories, which are single-image based method [4, 5, 8, 11, 12, 17, 30, 34] and multi-frame based method [2, 6, 7, 10, 20, 28, 31, 36].

For the single-image based methods, some of the early work [4, 8, 11, 17, 29, 34] are mainly used to enhance the quality of JPEG compressed images, which can also be applied directly to compressed videos to process each frame independently. [5, 12, 30] utilize certain characteristics of the video compression algorithm or compression parameters to improve the video quality. For example, DS-CNN [30] and QE-CNN [29] use distinct models to enhance the video processed by different compression coding.

For the multi-frame based methods, MFQE 1.0 [31] and MFQE 2.0 [10] were proposed to use two adjacent high quality frames(PQF) and compute the opti-

cal flow between them to enhance the current frame. STDF [6] uses deformation convolution for an implicit alignment. RFDA [36] extracts long-range temporal information from the video via the recursive fusion module. BasicVSR [1] and BasicVSR++ [2] utilize a bidirectional propagation network and a new alignment scheme is proposed in BasicVSR++. All these methods demonstrate the significance of temporal information for solving the compressed VQE problem.

As far as we know, there is still no compression VQE method for online scenario that has been proposed so far. The above-mentioned methods cannot be directly applied to webcasting environments due to the limitations of the two online restriction mentioned above.

**Look-up Table.** Look-up Tables (LUTs) have proven to be highly effective in reducing computational power and time consumption during the inference phase of algorithms by replacing complex computation with fast storage space retrieval operations. However, the use of LUTs directly is not always flexible as it requires manual adjustment by experts to accurately process images. To overcome this limitation, recent attempts have been made to improve LUTs. [25, 33] combine multiple LUTs and learn the weights through neural networks to summing up these LUT results. SR-LUT [13] replaces a small receptive field neural network with a 4D-LUT and achieves good speed-performance trade-offs on SR tasks. SP-LUT [21] and MuLUT [16] makes improvements to the SR-LUT by expanding its receptive field through parallel and serial multiple LUT tables. In this work, we utilize LUTs to extract information in both temporal and spatial dimensions, bringing its advantages to the online VQE task.

### 3 Method

#### 3.1 Overview

Given a stream of compressed frames without an explicit ending  $\{x_0, \dots, x_i, \dots\}$ , where  $x_i \in \mathbb{R}^{C \times H \times W}$  with input channel  $C$ , height  $H$  and width  $W$ , we sequentially enhance each compressed frame to obtain the target sequence  $\{y_0, \dots, y_i, \dots\}$ . Due to the low latency requirement of Online-VQE, obtaining information from future frames to enhance  $x_i$  is unacceptable. We only use past and current frames  $\{x_0, x_1, \dots, x_i\}$  to predict  $y_i$ , reducing the video’s delay time. Additionally, to avoid stuttering issues, each frame’s inference speed must be fast enough.

The overall flow of our proposed network during inference period is illustrated in Fig. 2 (The difference between the training and the inference phase is illustrated in Subsec. 3.4 and the figure in appendix). First, a Module-Agnostic Feature Extractor (MAFE) is utilized to extract the feature  $Feat_i$  of the current enhancing frame  $x_i$  as follows,

$$Feat_i = MAFE(x_i), \quad (1)$$

where the  $Feat_i$  will be shared by the three subsequent modules, thus reducing the multiple time-consuming extraction steps and fully exploiting the latent frame feature.

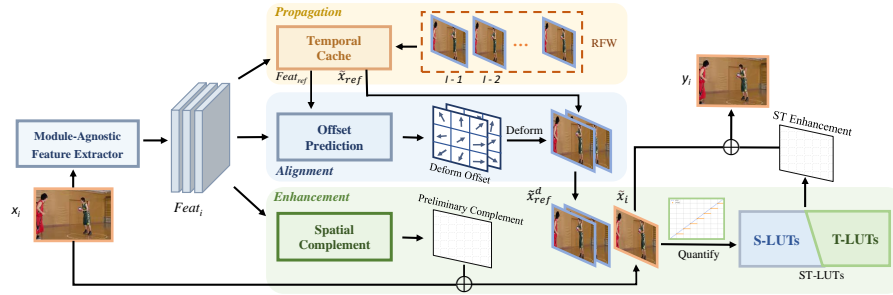


**Fig. 2:** The framework of STLQVE (inference phase), which consists of a Module-Agnostic Feature Extractor and three main parts: the propagation, alignment and enhancement module. In the inference phase, the propagation module selects the reference frame and accesses the relevant information, which is sent to the alignment module for temporal alignment, and finally the aligned reference frames and enhancing frame are input to the enhancement module for the final results.

Specifically, in the propagation module,  $Feat_i$  is stored in a structure called Temporal Cache, which will provide the temporal information in subsequent modules based on the selection of the reference frames  $x_{ref} = \{x_{ref1}, x_{ref2}\}$  without external computation. In the alignment module,  $Feat_i$  is concatenate with  $Feat_{ref}$ , the reference frame feature obtained from the propagation module, to deform  $x_{ref}$  with a lightweight offset predictor. In the enhancement module,  $Feat_i$  is used to perform a spatial complement, which fully exploits the extracted features and augments the ST-LUTs by increasing its receptive fields.

Under our proposed new framework, only once feature extraction computation for a single frame is required for enhancing each frame. The extracted features are simultaneously computed with reference frame alignment and preliminary compensation in the current frame space.

### 3.2 The Propagation Module

The propagation module in the VQE task is responsible for extracting and transmitting temporal information within the video. Previous methods have explored various approaches, including designing additional structures [10] and increasing the number of selected reference frames [6, 36] to improve network performance, which greatly increase inference time and computational costs of the model. The architecture of the propagation module is illustrated in Fig. 3. The compression configuration parameter quantization parameter (QP) value is utilized as an indicator to select fewer but higher quality frames among multiple candidate frames without extra computation. Specifically, a Reference Frame Window (RFW) which contains  $W$  frames  $\{x_{i-W}, \dots, x_{i-1}\}$  is set. Then, two frames with the smallest QP values are selected as  $x_{ref}$  for the subsequent module.

To mitigate the issue of additional feature extraction operations in previous works, we introduce a cache-like structure known as the Temporal Cache (TC).

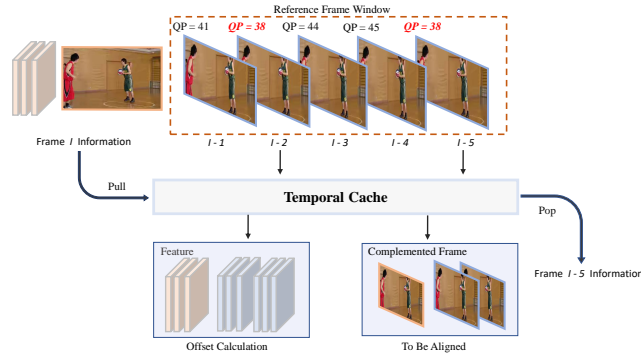


**Fig. 3:** Reference Frame Window and Temporal Cache in the propagation module.

The TC stores reusable features of past frames that were already extracted by the MAFE in previous process, thereby eliminating the need to re-extract features for each subsequent frame. In particular, when enhancing the  $i$ -th frame  $x_i$ , STLVE caches the intermediate feature map  $Feat_i$  extracted by the alignment module, as well as the enhanced frame, in the information cache (TC). During reference frame selection, the features and enhanced result of  $x_{ref1}$  and  $x_{ref2}$  are directly retrieved from TC without extra feature extraction process.

### 3.3 The Alignment Module

The alignment module is a crucial component in video processing tasks that handles spatial misalignments between frames, which plays a vital role in effectively utilizing the temporal information embedded in the video, especially when the video content is subject to large motion. STLVE includes a lightweight offset predictor to replace the optical flow or non-local computation of most VQE methods, which significantly reduce the computation cost.

The offset predictor is responsible for predicting spatial offsets which align correlated pixels in the reference with pixels in  $\tilde{x}_i$ . As introduced in the last section, the latent features  $Feat_{ref}$  and spatially compensated frames  $\tilde{x}_{ref}$  at each processing step are stored in TC, which are retrieved by RFW to enhance future frames. Given the feature of a reference frame  $\tilde{x}_{ref}$  retrieved from the TC, as well as the feature of the current frame  $\tilde{x}_i$ , the offset predictor predicts 9 spatial offsets for each pixel in  $\tilde{x}_i$ :

$$o_{ref} = C_{offset}([Feat_i, Feat_{ref}^d]) \quad (2)$$

where the matrix concatenation is denoted by  $[\cdot]$ , and each offset value in  $o_{ref}$  represents the position shift of a correlated pixel in  $\tilde{x}_{ref}$  relative to a pixel in  $\tilde{x}_i$ .

The temporal corresponding pixels in the reference frames  $x_{ref}$  are spatially aligned with the  $3 \times 3$  pixel offsets  $o_{ref}$  and bilinear interpolation. Each set of obtained correlated pixel values of a pixel in  $\tilde{x}_i$  are re-arranged into a  $3 \times 3$

patch, which are then stacked together to obtain the deformed reference frame denoted as  $\tilde{x}_{ref}^d$  with the size of  $N \times C \times 3H \times 3W$ .

### 3.4 The Enhancement Module

The enhancement module contains a spatial compensation network and a ST-LUTs network. To fully utilize the sharing latent feature  $Feat_i$ , a spatial compensation network reuses  $Feat_i$  to generate a spatial residual, which compensates the low quality frame  $x_i$  to obtain preliminary spatial enhancement before ST-LUTs:

$$\tilde{x}_i = x_i + C_{comp}(Feat_i) \quad (3)$$

where  $C_{comp}$  are 3 shallow convolutional layers. Since the subsequent enhancement module takes the obtained compensated frame  $\tilde{x}_i$  as input, spatial compensation network can boost the enhancement performance by expanding the receptive field of the ST-LUTs in the enhancement module. To match the resolution of  $\tilde{x}_{ref}^d$ ,  $\tilde{x}_i$  is upsampled by repeating each pixel in  $\tilde{x}_i$  to form a 3x3 patch, then each pixel in the up-sampled  $\tilde{x}_i$  is correlated with the pixel at the same position in  $\tilde{x}_{ref}^d$ . This is achieved by the unfold and fold operations with different strides as follows:

$$\tilde{x}_i^{up} = Fold(Unfold(\tilde{x}_i, stride = 1), stride = 3), \quad (4)$$

the up-sampled input frame  $\tilde{x}_i^{up}$  and deformed reference frame  $\tilde{x}_{ref}^d$  together serve as the input of the ST-LUTs network for the final quality enhancement.

Instead of deep neural network, STLVQE adopts a novel Spatial-Temporal Look-up Tables in the enhancement module during inference to replace complex convolutional computation used in training stage with much faster direct memory access, and conducts table queries on both spatial and temporal perspective.

**Quantization.** Due to the limited storage space of the LUT, the size of each pixel in the input compensated frame  $\tilde{x}_i^{up}$  and the deformed frames  $\tilde{x}_{ref}^d$  needs to be controlled to fit within a suitable range of bits. Because the range of values in  $\tilde{x}_i^{up}$  and  $\tilde{x}_{ref}^d$  can vary dynamically and the gradient needs to be passed through the quantization operation during end-to-end training, it's not practical to simply quantize the matrices using a fixed quantization hyper-parameter. The enhancement module adopts a Learnable Quantization layer (LSQ) [9] to quantize the input of the enhancement module as follows:

$$\bar{x} = \lfloor clip(\tilde{x}/s, -Q_N, Q_P) \rfloor, \quad \hat{x} = \bar{x} \times s, \quad (5)$$

where  $clip(z, r_1, r_2)$  returns matrix  $z$  with values below  $r_1$  set to  $r_1$  and values above  $r_2$  set to  $r_2$ , and the  $\lfloor z \rfloor$  rounds  $z$  to the nearest integer. The step size parameter  $s$  can be optimized along with the network's training.  $\bar{x}$  is the indexes used in the LUTs store and retrieval stages, and  $\hat{x}$  is a quantized representation of the data with the same scale as  $x$ . After quantization, the deep enhancement network and the corresponding LUTs can be constructed with the quantized pixel values as input.

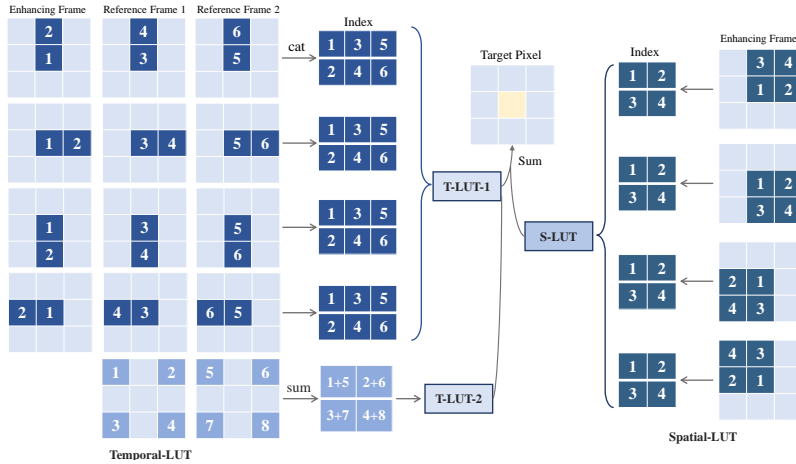


**Fig. 4:** The specific schematic of our Spatial-Temporal Look-up Tables, which consists of two parts: Temporal-LUT (left side) and Spatial-LUT (right side).

**Deep Enhancement Network Training.** In the training phase, a neural network based enhancement module is optimized, which takes the compensated frame  $\hat{x}_i^{up}$  and reference frames  $\hat{x}_{ref}^d$  as input and output the final enhancement results. To train an enhancement network that is suitable for LUT conversion, the receptive field size of the deep network typically cannot exceed 6 (Larger receptive fields will result in a higher storage occupancy, refer to the appendix for details). Therefore, each branch of the enhancement network, which will be replaced by ST-LUTs during the inference stage, consists of 1 convolutional layer with a kernel size of 4 or 6 and 10 convolutional layers with  $1 \times 1$  kernel. The specific design of the network will be illustrated in the appendix.

**ST-LUTs Construction & Replacement.** We generate LUTs by permuting all input patches of the receptive field size, and storing all the input/output mappings of the trained deep enhancement network in mapping tables. During inference, we retrieve the outputs of the deep enhancement network directly from the LUTs, replacing slow and computationally-intensive convolution with faster memory access and retain the other components in STLVQE. Due to the input patch size restriction, conventional LUTs are not suitable for inter-frame queries in the temporal dimension. To address these issues, we firstly propose the ST-LUTs, which employ multiple LUTs to conduct parallel retrieval with different sets of query pixels in both spatial and temporal dimensions.

Specifically, given the quantized compensated frames  $\hat{x}_i^{up}$  and the aligned frames  $\hat{x}_{ref}^d$  as input, the look-up tables are constructed as shown in Fig. 4, where two sets of LUTs named S-LUTs and T-LUTs are constructed for extracting spatial and temporal information respectively.

For S-LUTs, a rotation ensemble operation [13] is used during the training process to further expand the LUT receptive field. As shown in Fig. 4, during training, input images are rotated by 0, 90, 180, and 270 degrees, and the results



are reverse-rotated and summed up. This approach considers all pixels in a  $3 \times 3$  receptive field simultaneously. The result of S-LUT  $R_i^S$  is expressed as follows:

$$R_i^S = \frac{1}{4} \sum_{j=0}^4 Rot_j^{-1}(f^S(Rot_j(\hat{x}_i^{up}))), \quad (6)$$

where  $Rot_j$  and  $Rot_j^{-1}$  are the rotation and reserve-rotation operations, and  $f^S$  is the spatial enhancement network or the S-LUTs retrieval.

For T-LUTs, the pixels at the same location of the enhancing and reference frames will be strongly correlated after alignment, and jointly considering these values can make full use of the temporal information in the video. As shown on the left in Fig. 4, we establish two T-LUTs: T-LUT-1 take the same position pixels of  $\hat{x}_i^{up}$  and  $\hat{x}_{ref}^d$  as index with the rotation ensemble operation, while T-LUT-2 uses the four edge pixels of each kernel in the  $\hat{x}_{ref}^d$  as indexes to retrieve the surrounding information of the target pixels. The result of T-LUTs  $R_i^T$  can be expressed as follows:

$$\begin{aligned} R_i^{T1} &= \frac{1}{4} \sum_{j=0}^4 Rot_j^{-1}(f^{T1}(Rot_j([\hat{x}_i^{up}, \hat{x}_{ref}^d]))), \\ R_i^{T2} &= f^{T2}(\hat{x}_{ref}^d), \quad R_i^T = R_i^{T1} + R_i^{T2}, \end{aligned} \quad (7)$$

where  $f^{T1}$  and  $f^{T2}$  are the temporal enhancement network or the T-LUTs retrieval. Then we can acquire the results of ST-LUTs and get the final enhanced image  $y_i$  as follows:

$$R_i = R_i^S + R_i^T, \quad y_i = \tilde{x}_i + R_i. \quad (8)$$

### 3.5 Training Scheme

We perform the training of the STLVE in two stages with an end-to-end fashion. Firstly, the Charbonnier Loss [3] is utilized to optimize the model as follows:

$$L_{char} = \sqrt{(y_t - \bar{y}_t)^2 + \epsilon}, \quad (9)$$

where  $y_t$  and  $\bar{y}_t$  is the enhanced and ground truth frame at time  $t$ , and  $\epsilon$  is set to  $10^{-6}$  in our paper. Secondly, to further enhance the enhancement capability, we perform fine-tuning using L2 loss with a smaller learning rate as follows:

$$L_{MSE} = \|(y_t - \bar{y}_t)^2\|_2. \quad (10)$$

## 4 Experiments

### 4.1 Datasets

Following [6, 10, 36], we conduct our experiments on the MFQE 2.0 dataset. It contains totally 126 sequences videos with multi resolutions: SIF( $352 \times 240$ ),

**Table 1:** Overall comparison for  $\Delta$  PSNR(dB),  $\Delta$  SSIM( $\times 10^{-2}$ ), Latency(ms) and FPS over test sequences of MFQE 2.0 Dataset at QP=37. All methods were retested on a NVIDIA RTX 3090 in frame-to-frame manner. Video resolution: Class A(2560 $\times$ 1600), Class B(1980 $\times$ 1080), Class C(832 $\times$ 480), Class D(416 $\times$ 240), Class E(1280 $\times$ 720).

Approach	High-Latency VQE Methods						Low-Latency VQE Methods									
	MFQE 1.0 [31]		FSTQE [7]		Li et al. [17]		DS-CNN [29]		DnCNN [34]		DCAD [26]		STLVQE(Ours)			
Metrics	$\Delta P/\Delta S$	LT/FPS	$\Delta P/\Delta S$	LT/FPS	$\Delta P/\Delta S$	LT/FPS	$\Delta P/\Delta S$	LT/FPS	$\Delta P/\Delta S$	LT/FPS	$\Delta P/\Delta S$	LT/FPS	$\Delta P/\Delta S$	LT/FPS		
A Traffic	0.50/0.90	1120.1	0.64/1.04	5.6K	0.29/0.60	385.5	0.29/0.60	374.6	0.24/0.57	294.9	0.31/0.67	153.7	0.41/0.94	96.3		
PeopleOnStreet	0.80/1.37	1.0	1.08/1.68	0.2	0.48/0.92	2.6	0.42/0.85	2.7	0.41/0.82	3.4	0.50/0.95	6.5	0.68/1.35	10.4		
B Kimono	0.50/1.13		0.69/1.36		0.28/0.78		0.25/0.75		0.24/0.75		0.28/0.78		0.38/1.05			
ParkScene	0.39/1.03	628.1	0.49/1.21	2.9K	0.15/0.48	192.8	0.15/0.50	178.2	0.14/0.50	145.4	0.16/0.50	77.5	0.33/0.80	48.6		
Cactus	0.44/0.88	2.0	0.62/1.15	0.4	0.23/0.58	5.2	0.24/0.58	5.6	0.20/0.48	6.9	0.26/0.58	12.9	0.43/0.85	20.6		
BQTerrace	0.27/0.48		0.50/0.87		0.25/0.48		0.26/0.48		0.20/0.38		0.28/0.50		0.42/0.83			
BasketballDrive	0.41/0.80		0.60/1.04		0.30/0.68		0.28/0.65		0.25/0.58		0.31/0.68		0.49/1.00			
C RaceHorses	0.34/0.55		0.40/0.88		0.28/0.65		0.27/0.63		0.25/0.65		0.28/0.65		0.39/0.94			
BQMall	0.51/1.03	229.8	0.74/1.44	611.6	0.33/0.88	39.5	0.33/0.80	36.7	0.28/0.68	26.3	0.34/0.88	14.3	0.50/1.25	11.5		
PartyScene	0.22/0.73	10.4	0.51/1.46	1.8	0.13/0.45	25.3	0.17/0.58	27.2	0.13/0.48	38.0	0.16/0.48	69.9	0.34/1.15	87.0		
BasketballDrill	0.48/0.90		0.66/1.27		0.38/0.88		0.35/0.68		0.33/0.68		0.39/0.78		0.57/1.37			
D RaceHorses	0.51/1.13		0.60/1.44		0.33/0.83		0.32/0.75		0.31/0.73		0.38/0.83		0.44/1.08			
BQSquare	-0.01/0.15	164.3	0.79/1.14	203.7	0.09/0.25	24.3	0.20/0.38	12.1	0.13/0.18	7.0	0.20/0.38	3.5	0.37/0.75	9.1		
BlowingBubbles	0.39/1.20	32.2	0.62/1.95	7.3	0.21/0.68	41.2	0.23/0.68	82.6	0.18/0.58	142.9	0.22/0.65	285.7	0.37/1.23	109.9		
BasketballPass	0.63/1.38		0.85/1.75		0.34/0.85		0.34/0.78		0.31/0.75		0.35/0.85		0.48/1.28			
E FourPeople	0.66/0.85	345.4	0.95/1.12	1.3K	0.45/0.70	87.4	0.46/0.70	81.6	0.39/0.60	64.8	0.51/0.78	34.3	0.69/1.02	24.7		
Johnny	0.55/0.55	4.7	0.75/0.85	0.8	0.40/0.60	11.4	0.38/0.40	12.3	0.32/0.40	15.4	0.41/0.50	29.2	0.93/0.64	40.5		
KristenAndSara	0.66/0.75		0.93/0.91		0.49/0.68		0.48/0.60		0.42/0.60		0.52/0.70		0.74/0.84			
Average	0.46/0.88	-	0.69/1.25	-	0.30/0.66	-	0.30/0.63	-	0.26/0.58	-	0.32/0.67	-	0.49/1.03	-		

CIF(352  $\times$  288), NTSC(720  $\times$  486), 4CIF(704  $\times$  576), 240P(416  $\times$  240), 360P(640  $\times$  360), 480P(832  $\times$  280), 720P(1280  $\times$  720), 1080P(1920  $\times$  1080) and WQXGA (2560  $\times$  1600). Same as [10], the 108 videos in the dataset are used as the training set and 18 videos are used as the test set. All videos were compressed by HM16.5 software in LDP mode with QP values of 22, 27, 32, 37 and 42.

## 4.2 Implementation Details

Our proposed network is implemented based on PyTorch framework and MMEdit-ing toolbox [23]. During the training phase, we set batch size to 8 with 180 $\times$ 180 clips from the raw videos and the corresponding compressed videos as training samples. The random flip and rotation augmentation are utilized to fully exploit the information in the samples. The Adam optimizer [14] and Cosine Annealing scheme [19] are utilized for optimizing. The total iterations numbers and initial learning rate of the first and second stages is set to 200K,  $1 \times 10^{-4}$  and 100K,  $1 \times 10^{-6}$ . Our network is trained on 8 Telsa V100 GPUs.

During the inference phase, ST-LUTs will replace the corresponding convolutional layers. To evaluate the model’s performance in an online setting, we conduct inference on the test set frame-by-frame. Following the same settings as [10], we report quality enhancement on Y-channel in YUV/YCbCr space. The Peak Singal-to-Noise Ratio( $\Delta$ PSNR) and Structural Similarity( $\Delta$ SSIM) will be used as metrics to judge the model’s enhancement capability. We further evaluate the latency(LT) and frame per second(FPS) of the models which is crucial to the online-VQE:

$$LT = T_{process} + T_{wait}, \quad T_{wait} = N_f/FPS, \quad (11)$$

where  $T_{process}$  refers to the single-frame inference time and  $T_{wait}$  refers to the future frames waiting time required for some video based methods,  $N_f$  represent

**Table 2:** Latency on 720P video and averaged  $\Delta$ PSNR/ $\Delta$ SSIM comparison on the test sequences of MFQE 2.0 Dataset at different QP values. FV-Required means the full compressed video is required for enhancement, thus latency cannot be calculated.

Method	Type	LT(ms)	Storage	GFLOPs	QP37	QP42	QP32	QP27	QP22
MFQEv1 [31]	Bi-MF	345.4	1788K	-	0.46/0.88	0.44/1.30	0.43/0.58	0.40/0.34	0.31/0.19
MFQEv2 [10]	Bi-MF	320.1	255K	788	0.56/1.09	0.59/1.65	0.52/0.68	0.49/0.42	0.46/0.27
STDF [6]	Bi-MF	85.6	487K	293	0.65/1.18	-/-	0.64/0.77	0.59/0.47	0.51/0.27
PSTQE [7]	Bi-MF	1249.8	218K	679	0.69/1.25	0.69/1.86	0.67/0.83	0.63/0.52	0.55/0.29
RFDA [36]	Bi-MF	312.8	1250K	-	0.91/1.62	0.82/2.20	0.87/1.07	0.82/0.68	0.76/0.42
BasicVSR++ [2]	Bi-MF	FV-Required	7300K	423	0.95/1.80	-/-	0.89/1.25	-/-	-/-
RNAN [35]	SF	4329.4	8960K	6979	0.44/0.95	-/-	0.41/0.62	-/-	-/-
ARCNN [8]	SF	25.1	118K	108	0.23/0.45	0.29/0.96	0.18/0.19	0.18/0.14	0.14/0.08
DnCNN [34]	SF	64.8	558K	516	0.26/0.58	0.22/0.77	0.26/0.35	0.27/0.24	0.29/0.18
DS-CNN [29]	SF	81.6	948K	437	0.30/0.63	0.31/1.01	0.27/0.38	0.27/0.23	0.25/0.15
Li et al. [17]	SF	87.4	464K	434	0.30/0.66	0.32/1.05	0.28/0.37	0.30/0.28	0.30/0.19
DCAD [26]	SF	34.3	299K	275	0.32/0.67	0.32/1.09	0.32/0.44	0.32/0.30	0.31/0.19
STLVQE	Uni-MF	<b>24.7</b>	398K+228M	<b>98</b>	<b>0.49/1.03</b>	<b>0.50/1.60</b>	<b>0.45/0.64</b>	<b>0.41/0.40</b>	<b>0.34/0.24</b>

the number of future frames used. Note that the LT metric ignores the frame reception and decoding time, which is fair for different methods, and we set  $FPS=30$  in Eq. 11 as the general online video standard to facilitate comparison.

### 4.3 Comparison with State of the art Methods

In this subsection, we present the results of our extensive experiments on various QP compressed videos in Tab. 1 and Tab. 2. Our proposed STLVQE network is compared with some widely used or state-of-art single-frame methods [8, 17, 26, 29, 34, 35], as well as some efficient multi-frame methods [6, 7, 10, 31]. In online environment where video is streamed in real-time, Bi-direction Multi-Frame (Bi-MF) method necessitates waiting for future frames that have not yet been received in current time. This waiting period introduces uncontrollable latency to the stream. Consequently, as outlined in previous online works [18, 22, 32], the Bi-MF method can not be directly applied to online scenarios and is predominantly utilized for offline processing. As a result, both Bi-MF and slow single frame methods ( $>100$ ms) are placed in the first part in Tab. 1 and Tab. 2 for performance comparison, and demonstrate our favorable trade-off between performance and inference speed. All experiments were conducted on an NVIDIA RTX 3090 using a frame-to-frame style.

**Latency and FPS.** Tab. 1 presents the latency and FPS metrics for each VQE approach. We note that while low-latency VQE methods can process each frame at a lower latency and reduce video delay, they often struggle to handle high-resolution videos in real-time, which can lead to stuttering and reduced smoothness. Among the methods listed, only STLVQE can achieve FPS above 40 on 720P resolution videos, making it suitable for most online scenarios. Compared to the second fastest method DCAD, STLVQE’s processing time on 720p video is 9.6 milliseconds faster and outperforms it by a considerable margin, improving PSNR and SSIM metrics by 0.17dB and  $0.36 \times 10^{-2}$ , respectively.

Tab. 2 shows the latency of some large-scale high-latency temporal VQE methods. In contrast, high-latency VQE methods require waiting for future

**Table 3:** Ablation study of Temporal Cache(TC), Reference Frame Window(RFW), Deform Operation(DF), and Preliminary Complement Residual(PC). The latter three sections share the features extracted by MAFE.

RFW	TC	DF	PC	$\Delta P/\Delta S$	Time	Params(K)
✓	✓			0.06/0.01	10.85	<1
✓	✓	✓		0.31/0.51	21.85	352
✓	✓		✓	0.39/0.87	20.12	149
✓		✓	✓	0.49/1.03	45.61	398
		✓	✓	0.46/0.98	24.32	398
✓	✓	✓	✓	0.49/1.03	24.65	398

frames or taking a long time for inference, which can cause uncontrollable video delay. The latency of the two high-latency methods in Tab. 1 we evaluated exceeds 400ms, much higher than the latency caused by STLVQE. Moreover, when considering only the FPS metric, STLVQE achieves a significantly faster speed than the single-frame VQE method RNAN(FPS = 0.2) by a factor of 175 on 720P video. Compared with MFQE 1.0, our method is 8.6 times faster with a better enhancement performance. Additionally, STLVQE has a more significant speed advantage on higher resolution videos such as 1080P and 2K.

**Enhancement performance.** In Tab. 1 and Tab. 2, we present the performance of STLVQE compared to other commonly used or sota VQE methods for each video at QP=37 and for different QP compressed videos, respectively. Our method outperforms all the listed low-latency methods. In comparison with the high-latency VQE method, STLVQE reaches higher level with RNAN at QP=37 and QP=32, with only 2.6% and 0.6% of RNAN’s number of parameters and latency time (720P), respectively. The  $\Delta SSIM$  of STLVQE is higher than that of the MFQE method for all five QPs, indicating that our method produces an enhanced image with a more stable image structure. The specific visualization results and analysis can be found in *Qualitative Comparison* section. STDF is a robust VQE method, but we believe that a stable latency and higher frame rate are more important for enhancing the user’s viewing experience.

**Memory Size & GPU Consumption.** As shown in Tab. 2, STLVQE has space occupation of 398KB for the model and 228MB for the LUT(utilizing less than 5% memory of a low end GPU like GTX 1060), achieving real-time processing capability. Since most deep networks are replaced with ST-LUTs, inferencing STLVQE only needs 98 GFLOPs on a 720P frame. Note that GPU computing unit are more expensive than the memory.

#### 4.4 Ablation Study

To validate the effectiveness of our proposed new VQE framework, we perform ablation experiments and specific analysis on three components. The results of the runtime per frame is computed on 720P videos at QP = 37.

**Effectiveness of the propagation module.** The results are shown in the 5th and 6th row of Tab. 3. We found that selecting frames based on QP val-

**Table 4:** Ablation study of STLUTs and the CNN enhancement network. The runtime is computed on a 720P video.

Enhancement Module	$\Delta P/\Delta S$	Time(ms)	Params(K)
S-LUT	0.39/0.83	23.52	398
S-LUT + T-LUT-1	0.45/1.02	24.12	398
ST-LUTs	0.47/1.02	24.65	398
ST-LUTs (on $\tilde{x}_i$ )	0.49/1.03	24.65	398
CNN Network	0.50/1.08	147.02	442

ues in RFW can bring a 0.03dB  $\Delta$ PSNR performance improvement compared to randomly selecting frames in the RFW, without adding parameters to the network and only increasing the inference time by 0.33 ms for comparing QP values of each frame. Furthermore, as shown in rows 4 and 6 of Tab. 3, the use of the TC structure can significantly reduce the inference time by 21.0 ms, which is consumed by the repeated computation of the reference frame information. We achieve this reduction in time by merely occupying the GPU memory with information of several frames in the RFW.

**Effectiveness of the alignment module.** We mainly validate the effect of the deform operation of the reference frame in the Alignment module. As shown in the first row of Tab. 3, when only using the ST-LUTs structure and discard the whole alignment module and PC operation, the result only has a 0.06 dB PSNR improvement compared to HEVC video. When the Deform operation is applied, the network can capture more accurate temporal information, and the  $\Delta$ PSNR reaches 0.31 dB. Due to the lightweight convolutional layers, the alignment module only adds 11.6 ms of inference time to the network.

**Effectiveness of the enhancement module.** As shown in row 3 of Tab. 3, using PC without the Deform operation achieves a significant  $\Delta$ PSNR of 0.39 dB, demonstrating the effectiveness of PC in providing initial compensation for spatial information and extending the receptive field, ultimately enhancing the performance of ST-LUTs. Finally, after combining two parts, the network achieves 0.49 dB  $\Delta$ PSNR. PC alone contributes 0.18 dB to the network and adds only 2.16 ms of inference time.

Tab. 4 provides an analysis of the impact of each LUT in the enhancement module. In the first three rows of the table, we attempted to enhance the original image  $x_i$  with the results of different LUT combinations. Results in the first and second rows show that using only the S-LUT with T-LUT-1 does not fully improve the network due to T-LUT-1 not utilizing all pixels within a kernel when learning the alignment offset. However, when T-LUT-2 is used for network training along with T-LUT-1, the reference frame can be better aligned, resulting in a  $\Delta$ PSNR improvement of 0.08 dB. The 4th row shows the enhancing result on  $\tilde{x}_i$ , reducing the learning difficulty of the ST-LUTs, which improving the performance by 0.02 dB. Compared to the CNN layers replaced by LUTs, ST-LUTs sacrifice only 0.01 dB  $\Delta$ PSNR performance while reducing the number of parameters by 44K and the inference time by 122.37 ms.

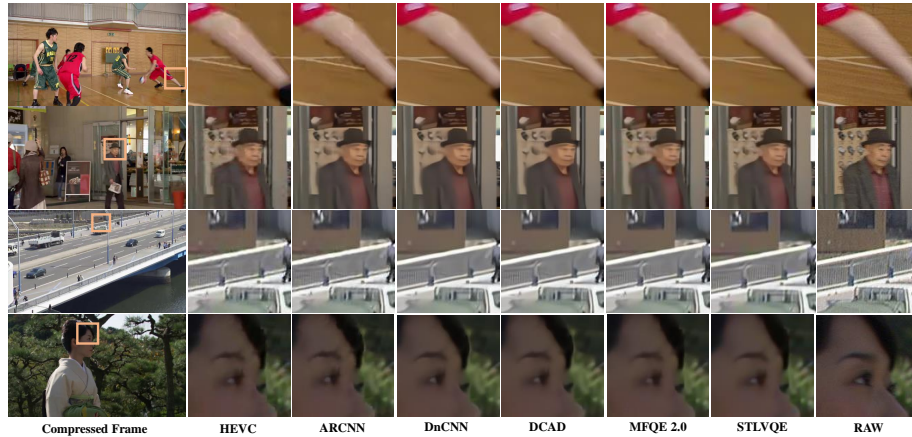


**Fig. 5:** Qualitative results at QP 37. The STLVQE method successfully enhances the left leg of the athlete, the face of the old man, the railings of the bridge and the eyebrow of the woman in each frame, respectively.

The above ablation studies have sufficiently demonstrated that the MAFE structure of shared features in STLVQE with the redesigned three new modules can sufficiently reduce the computational redundancy of the network and obtain satisfactory inference speed-performance trade-offs.

#### 4.5 Qualitative Comparison

Fig. 5 provides 4 examples of the qualitative results of our network on compressed video at  $QP=37$ . The quality of these images deteriorates significantly in compressed scenes, showing a variety of image defects (e.g. blurring legs, missing bridge railings). With the help of temporal information, STLVQE achieves better visual results than single-frame methods with significantly reduced runtime. Compared to large-scale multi-frame methods like MFQE 2.0, STLVQE can achieve competitive capabilities in detail and structural restoration.

## 5 Conclusion

In this paper, we propose a lightweight and rapid method called STLVQE based on the constraints of online video quality enhancement tasks. STLVQE greatly reduce the computation redundancy and uses a Spatial-Temporal Look-up Table structure to extract spatio-temporal information from the video with minimal time consumption. The extensive experiments prove that our proposed method can outperform most low-latency VQE methods, achieve competitive performance with high-latency VQE methods which cannot be directly utilized on Online-VQE tasks. Furthermore, STLVQE achieves real-time processing of 720P resolution videos, demonstrating a good trade-off between enhancement performance and inference speed.

## Acknowledgements

This work was supported by National Natural Science Fund of China (62076184, 61976158, 61976160, 62076182, 62276190), in part by Fundamental Research Funds for the Central Universities and State Key Laboratory of Integrated Services Networks (Xidian University), in part by Shanghai Innovation Action Project of Science and Technology (20511100700) and Shanghai Natural Science Foundation (22ZR1466700).

## References

1. Chan, K.C., Wang, X., Yu, K., Dong, C., Loy, C.C.: Basicvsr: The search for essential components in video super-resolution and beyond. In: Proceedings of the IEEE/CVF Conference on Computer Vision and Pattern Recognition. pp. 4947–4956 (2021) [2](#), [3](#), [4](#)
2. Chan, K.C., Zhou, S., Xu, X., Loy, C.C.: Basicvsr++: Improving video super-resolution with enhanced propagation and alignment. In: Proceedings of the IEEE/CVF conference on computer vision and pattern recognition. pp. 5972–5981 (2022) [2](#), [3](#), [4](#), [11](#)
3. Charbonnier, P., Blanc-Feraud, L., Aubert, G., Barlaud, M.: Two deterministic half-quadratic regularization algorithms for computed imaging. In: Proceedings of 1st international conference on image processing. vol. 2, pp. 168–172. IEEE (1994) [9](#)
4. Chen, H., He, X., Qing, L., Xiong, S., Nguyen, T.Q.: Dpw-sdnet: Dual pixel-wavelet domain deep cnns for soft decoding of jpeg-compressed images. In: Proceedings of the IEEE Conference on Computer Vision and Pattern Recognition Workshops. pp. 711–720 (2018) [2](#), [3](#)
5. Dai, Y., Liu, D., Wu, F.: A convolutional neural network approach for post-processing in hevc intra coding. In: MultiMedia Modeling: 23rd International Conference, MMM 2017, Reykjavik, Iceland, January 4-6, 2017, Proceedings, Part I 23. pp. 28–39. Springer (2017) [3](#)
6. Deng, J., Wang, L., Pu, S., Zhuo, C.: Spatio-temporal deformable convolution for compressed video quality enhancement. In: Proceedings of the AAAI conference on artificial intelligence. vol. 34, pp. 10696–10703 (2020) [2](#), [3](#), [4](#), [5](#), [9](#), [11](#)
7. Ding, Q., Shen, L., Yu, L., Yang, H., Xu, M.: Patch-wise spatial-temporal quality enhancement for hevc compressed video. IEEE Transactions on Image Processing **30**, 6459–6472 (2021) [3](#), [10](#), [11](#)
8. Dong, C., Deng, Y., Loy, C.C., Tang, X.: Compression artifacts reduction by a deep convolutional network. In: Proceedings of the IEEE international conference on computer vision. pp. 576–584 (2015) [3](#), [11](#)
9. Esser, S.K., McKinsty, J.L., Bablani, D., Appuswamy, R., Modha, D.S.: Learned step size quantization. arXiv preprint arXiv:1902.08153 (2019) [7](#)
10. Guan, Z., Xing, Q., Xu, M., Yang, R., Liu, T., Wang, Z.: Mfqe 2.0: A new approach for multi-frame quality enhancement on compressed video. IEEE transactions on pattern analysis and machine intelligence **43**(3), 949–963 (2019) [2](#), [3](#), [5](#), [9](#), [10](#), [11](#)
11. Guo, J., Chao, H.: Building dual-domain representations for compression artifacts reduction. In: Computer Vision—ECCV 2016: 14th European Conference, Amsterdam, The Netherlands, October 11–14, 2016, Proceedings, Part I 14. pp. 628–644. Springer (2016) [3](#)

12. Jin, Z., An, P., Yang, C., Shen, L.: Quality enhancement for intra frame coding via cnns: An adversarial approach. In: 2018 IEEE International Conference on Acoustics, Speech and Signal Processing (ICASSP). pp. 1368–1372. IEEE (2018) [2](#), [3](#)
13. Jo, Y., Kim, S.J.: Practical single-image super-resolution using look-up table. In: Proceedings of the IEEE/CVF Conference on Computer Vision and Pattern Recognition. pp. 691–700 (2021) [3](#), [4](#), [8](#)
14. Kingma, D.P., Ba, J.: Adam: A method for stochastic optimization. arXiv preprint arXiv:1412.6980 (2014) [10](#)
15. Kondratyuk, D., Yuan, L., Li, Y., Zhang, L., Tan, M., Brown, M., Gong, B.: Movinets: Mobile video networks for efficient video recognition. In: Proceedings of the IEEE/CVF Conference on Computer Vision and Pattern Recognition. pp. 16020–16030 (2021) [2](#)
16. Li, J., Chen, C., Cheng, Z., Xiong, Z.: Mulut: Cooperating multiple look-up tables for efficient image super-resolution. In: Computer Vision–ECCV 2022: 17th European Conference, Tel Aviv, Israel, October 23–27, 2022, Proceedings, Part XVIII. pp. 238–256. Springer (2022) [4](#)
17. Li, K., Bare, B., Yan, B.: An efficient deep convolutional neural networks model for compressed image deblocking. In: 2017 IEEE International Conference on Multimedia and Expo (ICME). pp. 1320–1325. IEEE (2017) [3](#), [10](#), [11](#)
18. Lin, J., Gan, C., Han, S.: Tsm: Temporal shift module for efficient video understanding. In: Proceedings of the IEEE/CVF international conference on computer vision. pp. 7083–7093 (2019) [2](#), [11](#)
19. Loshchilov, I., Hutter, F.: Sgdr: Stochastic gradient descent with warm restarts. arXiv preprint arXiv:1608.03983 (2016) [10](#)
20. Lu, G., Ouyang, W., Xu, D., Zhang, X., Gao, Z., Sun, M.T.: Deep kalman filtering network for video compression artifact reduction. In: Proceedings of the European Conference on Computer Vision (ECCV). pp. 568–584 (2018) [2](#), [3](#)
21. Ma, C., Zhang, J., Zhou, J., Lu, J.: Learning series-parallel lookup tables for efficient image super-resolution. In: Computer Vision–ECCV 2022: 17th European Conference, Tel Aviv, Israel, October 23–27, 2022, Proceedings, Part XVII. pp. 305–321. Springer (2022) [4](#)
22. Maggioni, M., Huang, Y., Li, C., Xiao, S., Fu, Z., Song, F.: Efficient multi-stage video denoising with recurrent spatio-temporal fusion. In: Proceedings of the IEEE/CVF Conference on Computer Vision and Pattern Recognition. pp. 3466–3475 (2021) [2](#), [11](#)
23. MMEediting Contributors: MMEediting: OpenMMLab image and video editing toolbox. <https://github.com/open-mmlab/mmediting> (2022) [10](#)
24. Sullivan, G.J., Ohm, J.R., Han, W.J., Wiegand, T.: Overview of the high efficiency video coding (hevc) standard. IEEE Transactions on circuits and systems for video technology **22**(12), 1649–1668 (2012) [1](#)
25. Wang, T., Li, Y., Peng, J., Ma, Y., Wang, X., Song, F., Yan, Y.: Real-time image enhancer via learnable spatial-aware 3d lookup tables. In: Proceedings of the IEEE/CVF International Conference on Computer Vision. pp. 2471–2480 (2021) [4](#)
26. Wang, T., Chen, M., Chao, H.: A novel deep learning-based method of improving coding efficiency from the decoder-end for hevc. In: 2017 Data Compression Conference (DCC). pp. 410–419. IEEE (2017) [10](#), [11](#)
27. Wiegand, T., Sullivan, G.J., Bjontegaard, G., Luthra, A.: Overview of the h. 264/avc video coding standard. IEEE Transactions on circuits and systems for video technology **13**(7), 560–576 (2003) [1](#)



28. Xu, Y., Gao, L., Tian, K., Zhou, S., Sun, H.: Non-local convlstm for video compression artifact reduction. In: Proceedings of the IEEE/CVF international conference on computer vision. pp. 7043–7052 (2019) [3](#)
29. Yang, R., Xu, M., Liu, T., Wang, Z., Guan, Z.: Enhancing quality for hevc compressed videos. *IEEE Transactions on Circuits and Systems for Video Technology* **29**(7), 2039–2054 (2018) [2](#), [3](#), [10](#), [11](#)
30. Yang, R., Xu, M., Wang, Z.: Decoder-side hevc quality enhancement with scalable convolutional neural network. In: 2017 IEEE International Conference on Multimedia and Expo (ICME). pp. 817–822. IEEE (2017) [2](#), [3](#)
31. Yang, R., Xu, M., Wang, Z., Li, T.: Multi-frame quality enhancement for compressed video. In: Proceedings of the IEEE conference on computer vision and pattern recognition. pp. 6664–6673 (2018) [2](#), [3](#), [10](#), [11](#)
32. Yin, G., Qu, Z., Jiang, X., Jiang, S., Han, Z., Zheng, N., Yang, H., Liu, X., Yang, Y., Li, D., et al.: Online streaming video super-resolution with convolutional look-up table. *IEEE Transactions on Image Processing* **33**, 2305–2317 (2024) [11](#)
33. Zeng, H., Cai, J., Li, L., Cao, Z., Zhang, L.: Learning image-adaptive 3d lookup tables for high performance photo enhancement in real-time. *IEEE Transactions on Pattern Analysis and Machine Intelligence* **44**(4), 2058–2073 (2020) [4](#)
34. Zhang, K., Zuo, W., Chen, Y., Meng, D., Zhang, L.: Beyond a gaussian denoiser: Residual learning of deep cnn for image denoising. *IEEE transactions on image processing* **26**(7), 3142–3155 (2017) [3](#), [10](#), [11](#)
35. Zhang, Y., Li, K., Li, K., Zhong, B., Fu, Y.: Residual non-local attention networks for image restoration. arXiv preprint arXiv:1903.10082 (2019) [11](#)
36. Zhao, M., Xu, Y., Zhou, S.: Recursive fusion and deformable spatiotemporal attention for video compression artifact reduction. In: Proceedings of the 29th ACM international conference on multimedia. pp. 5646–5654 (2021) [2](#), [3](#), [4](#), [5](#), [9](#), [11](#)